



HAL
open science

The precursor phase of the CMR metallic state probed by spin and lattice dynamics

Martine Hennion, Fernande Moussa

► **To cite this version:**

Martine Hennion, Fernande Moussa. The precursor phase of the CMR metallic state probed by spin and lattice dynamics. *New Journal of Physics*, 2005, 7, pp.84. 10.1088/1367-2630/7/1/084 . cea-00162083

HAL Id: cea-00162083

<https://cea.hal.science/cea-00162083>

Submitted on 12 Jul 2007

HAL is a multi-disciplinary open access archive for the deposit and dissemination of scientific research documents, whether they are published or not. The documents may come from teaching and research institutions in France or abroad, or from public or private research centers.

L'archive ouverte pluridisciplinaire **HAL**, est destinée au dépôt et à la diffusion de documents scientifiques de niveau recherche, publiés ou non, émanant des établissements d'enseignement et de recherche français ou étrangers, des laboratoires publics ou privés.

The precursor phase of the CMR metallic state probed by spin and lattice dynamics

M Hennion and F Moussa

Laboratoire Léon Brillouin, CEA-CNRS, CE Saclay, 91191 Gif-sur-Yvette Cedex, France

E-mail: Martine.Hennion@cea.fr

New Journal of Physics 7 (2005) 84

Received 5 November 2004

Published 24 March 2005

Online at <http://www.njp.org/>

doi:10.1088/1367-2630/7/1/084

Abstract. The origin of the colossal magnetoresistance (CMR) observed in $\text{La}_{1-x}\text{Ca}_x\text{MnO}_3$, at $x \approx 0.3$, is still largely debated. Actually, the precursor phase of the ferromagnetic (F) metallic state, defined as the concentration ranges $0.125 \leq x_{\text{Ca}} < 0.22$ and $0.1 \leq x_{\text{Sr}} < 0.17$ in $\text{La}_{1-x}\text{Ca}_x\text{MnO}_3$ and $\text{La}_{1-x}\text{Sr}_x\text{MnO}_3$ systems respectively, is poorly understood. At these concentrations where the compounds are F, a very specific temperature behaviour is observed, the systems evolving from a quasi-metallic state below T_C towards an insulating state at lower temperatures. The double-exchange coupling alone is insufficient to describe the physics of these compounds and other interactions have to be considered, the origin of which is still unclear. In this paper, we mainly review and discuss neutron scattering studies performed on three compounds, $\text{La}_{0.83}\text{Ca}_{0.17}\text{MnO}_3$, $\text{La}_{0.875}\text{Sr}_{0.125}\text{MnO}_3$ and $\text{La}_{0.8}\text{Ca}_{0.2}\text{MnO}_3$. The magnetic excitations, as well as the dispersion of acoustic and lower optical phonons have been determined using inelastic neutron scattering. In the three systems, and over the whole temperature range, the spin-wave excitation spectrum is characterized by a splitting into several levels or several branches which are more or less dispersed. In the quasi-metallic state, particularly studied in the two Ca-doped compounds, these levels can be characterized as spin-waves confined within nanosize F spin domains. Within some model, a quantitative analysis of these excitations is proposed which determines their sizes, shapes and magnetic couplings. These couplings are found to be anisotropic, a feature characteristic of some orbital-ordering. These observations are interpreted by a charge segregation. Moreover, in the low-temperature state of $\text{La}_{0.83}\text{Ca}_{0.17}\text{MnO}_3$, the existence of an underlying periodicity for the magnetic characteristics is revealed, suggesting a charge-ordered state similar to the case of $\text{La}_{0.875}\text{Sr}_{0.125}\text{MnO}_3$. Finally, a coupling of magnons with acoustic and lower optical phonon branches is strongly suggested,

particularly in $\text{La}_{0.875}\text{Sr}_{0.125}\text{MnO}_3$, where a coincidence between the magnon and acoustic phonon energies is observed in a large q -range along the $[1\ 0\ 0]$ direction.

Contents

1. Introduction	2
1.1. Pure LaMnO_3	3
1.2. Low doping regime or CAF state	3
1.3. The CAF/F transition	5
1.4. The precursor F phase	6
1.5. Outline	6
2. Transport, structural and magnetic properties	7
2.1. Resistivity	7
2.2. Structural properties	7
2.3. Magnetic Bragg peaks	7
3. Phonon dispersion curves	11
3.1. $\text{La}_{0.8}\text{Ca}_{0.2}\text{MnO}_3$ and $\text{La}_{0.83}\text{Ca}_{0.17}\text{MnO}_3$	11
3.2. $\text{La}_{0.875}\text{Sr}_{0.125}\text{MnO}_3$	11
4. Spin-wave excitations	11
4.1. $\text{La}_{0.83}\text{Ca}_{0.17}\text{MnO}_3$	13
4.1.1. Spin-waves along $[1\ 0\ 0] + [0\ 1\ 0] + [0\ 0\ 1]$	13
4.1.2. Interpretation: confined spin-waves in two-dimensional F domains and charge ordering	15
4.2. $\text{La}_{0.875}\text{Sr}_{0.125}\text{MnO}_3$	17
4.2.1. Spin-waves along $[1\ 0\ 0] + [0\ 1\ 0] + [0\ 0\ 1]$ at $T = 15\ \text{K}$	17
4.2.2. Discussion	20
4.3. $\text{La}_{0.8}\text{Ca}_{0.2}\text{MnO}_3$	20
4.3.1. Spin-waves along $[1\ 0\ 0] + [0\ 1\ 0] + [0\ 0\ 1]$	21
4.3.2. Spin-waves along $[1\ 1\ 0]$ and $[1\ 1\ 1]$ at $T = 150\ \text{K}$	22
4.3.3. Discussion: confined spin-waves in 3D isotropic clusters	23
5. General discussion	25
Acknowledgments	26
References	26

1. Introduction

The phase diagram of doped manganites exhibits a variety of structural and magnetic phases which have attracted considerable attention in the last few years. The physical properties of these states are often sensitive to small changes in external conditions, giving rise to a number of ‘colossal effects’, among which is the colossal magnetoresistance (CMR). However, the very origin of this effect is still widely debated. A crucial point is actually that the precursor phase of the metallic ferromagnetic (F) phase itself is still poorly understood.

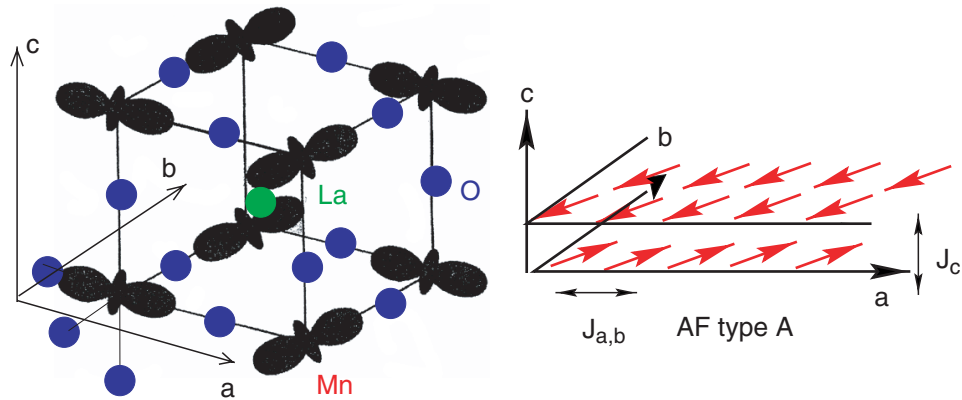


Figure 1. Orbital structure (left panel) and AF structure of type A (right panel) in LaMnO₃.

It is now clear that the double-exchange (DE) coupling alone [1] cannot explain the CMR properties. The most striking example is the existence of a non-metallic F phase at concentrations lower than those defining the metallic state, in both La_{1-x}Ca_xMnO₃ and La_{1-x}Sr_xMnO₃. Other mechanisms have been suggested such as electron-phonon coupling [2], charge segregation processes [3]–[7] with magnetic or lattice character (magnetic or lattice polarons), or orbital degeneracy effects [11]–[13], but their respective importance remains controversial.

The present paper is devoted to this peculiar F precursor phase, but we will start with a survey of known properties of the insulating phases at low-doping.

1.1. Pure LaMnO₃

The pure compound, LaMnO₃, is well understood. The Mn³⁺ ions have one electron in the $d_{3z^2-r^2}$ e_g orbital state, which induces a magnetic coupling of superexchange type. An antiferromagnetic (AF) structure of type A appears below $T_N = 140$ K, which consists of F (**a**, **b**) planes stacked antiferromagnetically along the **c** direction (figure 1, right panel). Here, **a**, **b**, **c** correspond to the axes of the pseudo-cubic structure of the perovskite. This magnetic structure derives from the orbital-ordered state (figure 1, left panel) which occurs at $T_{JT} = 750$ K and is associated with a structural transition from a pseudo-cubic to an orthorhombic phase [10]. The exchange interactions between the first Mn neighbours have been shown to be equal along **a** and **b**, with $J_{a,b} > 0$, and $J_c < 0$ from the q -dispersion of magnetic excitations [14, 15], and the experimental values are in good agreement with theory [21]. In addition, a large energy gap is observed at $q = 0$, indicating a large single-ion anisotropy, associated with the spin alignment along [**a** + **b**].

1.2. Low doping regime or CAF state

When increasing the hole doping, the first step ($0.05 < x_{Ca} < 0.125$, $0.05 < x_{Sr} < 0.1$) corresponds to a canted antiferromagnetic state (CAF), at low temperature, in agreement with de Gennes [8] mean field theory. With increasing x , the average F spin component is gradually rotated towards **c**. However, this magnetic state is inhomogeneous [16]. The inhomogeneities consist in small anisotropic magnetic clusters, which have been quantitatively characterized.

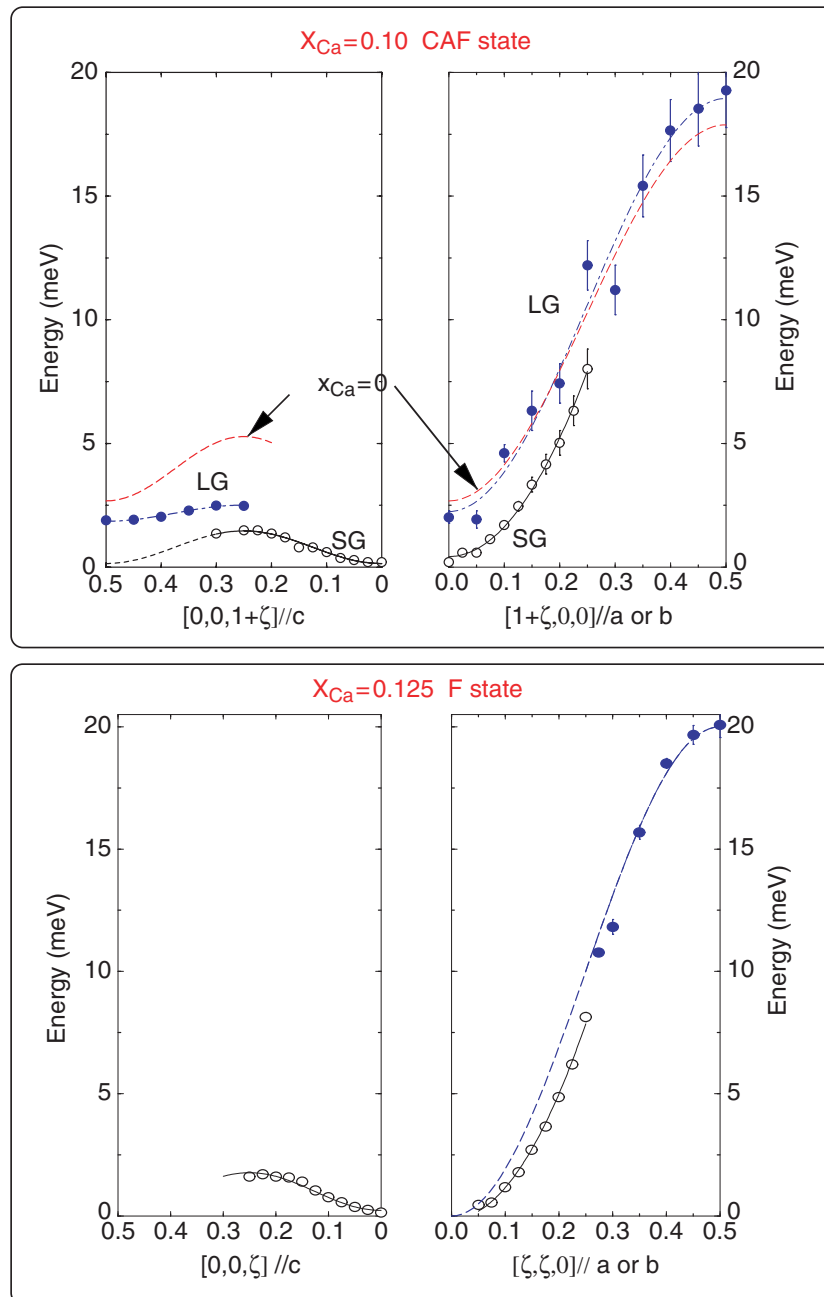


Figure 2. The large gap (LG, ●) and small gap (SG, ○) spin-wave branches in $\text{La}_{0.9}\text{Ca}_{0.1}\text{MnO}_3$ (upper panel) and in $\text{La}_{0.875}\text{Ca}_{0.125}\text{MnO}_3$ (lower panel).

They have a larger size ($\xi \approx 16 \text{ \AA}$) in the (a, b) plane than along c, the average distance between clusters is $d \approx 2\xi$. A distance of exclusion $d' \approx \xi$ indicates a repulsive interaction [17].

The nature of the CAF state was further characterized from the magnetic excitations or spin-waves, determined by inelastic neutron scattering [16]–[20]. Two spin-wave branches with distinct q -dependences have been observed. As an example, the spin-waves of the $x_{\text{Ca}} = 0.1$ compound are reported in figure 2 (upper panel), in cubic indexing for c (left panel) and a or

b (right panel) directions. One branch with a large anisotropy gap (LG), close to that of pure LaMnO_3 , has been modelled using a Heisenberg Hamiltonian, and its doping dependence denotes an increase with x of the F superexchange constant $J_{a,b}(x)$ and a decrease, in absolute value, of the AF $J_c(x)$ constant. Both variations are expected, due to the effect of F double-exchange coupling. They agree with the theoretical model of Feiner and Olés [21], although, in this model, a single branch is predicted. This branch with the large anisotropy gap is related to the magnetic characteristics of the matrix of Mn^{3+} ions, renormalized by the effect of DE. A second branch, induced by doping, is observed around F Bragg peaks only. It lies at lower energy, with a small gap (SG), and follows a quadratic dispersion in the small q -range, indicating an F character. However, its q -dependence is quite peculiar. Along **c**, it exhibits a $2a$ periodicity, characteristic of the AF order. Along **a** or **b**, it can be clearly identified only in the first half of the Brillouin zone. These features indicate a new F coupling, induced by mobile holes coupled by DE, on a distance of two or several lattice spacings through the hole-poor matrix of Mn^{3+} ions. The true origin of this coupling, which, as seen below, takes place in a large part of the phase diagram up to the metallic state ($x_{\text{Ca}} = 0.22$), is not known.

These two branches have well-defined dispersions and low damping, which demonstrates their coherent nature and thus points out that this CAF magnetic phase has a single ground state. This is in agreement with a picture of ‘charge segregation’ but not with that of ‘phase separation’.

1.3. The CAF/F transition

The next step towards the genuine metallic phase is a F phase, with very peculiar properties. It occurs at a critical value x_{cr} , with $x_{cr} = 0.125$ and 0.1 for Ca and Sr substitution, respectively, where the first signature of a ‘metallic’ behaviour is observed below T_C . This transition line corresponds precisely to the cancelling of the AF coupling J_c in the $J_c(x)$ variation obtained from the LG spin-wave branch [20]. As expected for an F state with one spin lattice, only one spin-wave branch is observed at this critical concentration. This is illustrated in figure 2 (lower panel), for $x_{\text{Ca}} = 0.125$, in cubic indexing. Referring to the previous step (figure 2, upper panel) the evolution from two branches towards one branch, may be described as follows. Along **c**, the LG branch observed around AF Bragg peaks, characteristic of the Mn^{3+} matrix, disappears with the AF peaks ($\tau = (0, 0, 0.5)$ in cubic indexing), and only the SG branch persists with very little change. It retains a ‘ $2a$ ’ periodicity along **c**, which is a very puzzling observation in such an F state. This will be further discussed below. In the (**a**, **b**) plane, the LG branch also disappears, at least for $q < 0.25$, e.g. for large wavelength. For $q > 0.25$ (short-wavelength spin-waves), the observed single branch is reminiscent of the ‘LG branch’ observed at $x < x_{cr}$. Actually, along **a** or **b**, the whole q -dispersion exhibits an ‘S’ shape with a small anomaly at $q = 0.25$, as observed also in another similar compound [9]. This description suggests that the magnetic excitations with $q < 0.25$ and > 0.25 correspond to a magnetic coupling of a distinct nature, similarly to the LG and the SG branches in the CAF state, and therefore that the magnetic state is still inhomogeneous. This evolution with x may be interpreted by a percolation process within the (**a**, **b**) planes, in agreement with theoretical predictions [22]. The matrix of Mn^{3+} ions associated with the LG branch, infinite for $x < x_{cr}$ (the LG branch exists at all q) would be broken on small scales ($q > 0.25$) by a new percolating quasi-metallic network. The specific scale ($q = 0.25$) indicated by the spin-wave branch in the (**a**, **b**) plane, could be related to the scale of an underlying charge segregation, undetected by magnetic diffuse scattering, probably because of insufficient magnetic contrast.

1.4. The precursor F phase

The anomalies in the transport, magnetic and structural properties which appear just beyond x_{cr} , are specific of the intermediate F phase, precursor of the F metallic state. Below T_C , a quasi-metallic state is defined by a decrease in the resistivity. At a lower temperature, a new transition occurs characterized by an increase in the resistivity with structural changes and magnetization anomalies [23]–[25]. This transition, which cannot be explained by DE, reveals the existence of additional interactions. The differences observed between the Sr- and Ca-doped systems points out a competition between such interactions.

In $\text{La}_{1-x}\text{Sr}_x\text{MnO}_3$ ($0.1 < x_{\text{Sr}} \leq 0.17$), weak superlattice Bragg peaks, $(h, k, l + 1/2)_{\text{cub}}$ and $(h, k, l + 1/4)_{\text{cub}}$ (in pseudo-cubic notation with $a_0 \approx 3.9 \text{ \AA}$ as the length of the cubic edge) appear at this transition [27, 28]. This has been interpreted as the occurrence of a charge ordering. This new phase has been extensively studied, experimentally [29]–[35], [38, 39] and theoretically [36, 37]. The origin of the transition has been attributed either to elastic forces [36] or to a new kind of orbital ordering [34, 39] or to a lattice polaron ordering [27], but no definitive conclusion has been reached so far.

In $\text{La}_{1-x}\text{Ca}_x\text{MnO}_3$, such superstructure peaks have not been reported up to now. In this system, short-range structural correlations have been found at $\mathbf{q} = (1/4, 1/4, 0)_{\text{cub}}$, and characterized as ‘correlated lattice polarons’ [40], as in the $x_{\text{Ca}} \approx 0.3$ metallic compound above T_C [41]. In the same compound, NMR [42] and Mossbauer spectroscopy [43] provide indications of an inhomogeneous state, whereas susceptibility measurements indicate irreversibilities and spin-glass properties [44].

In such a complex situation, it is of primary interest to investigate the elementary excitations of these systems. Spin-wave measurements have been recently reported in $\text{La}_{1-x}\text{Sr}_x\text{MnO}_3$ ($x = 0.9$ and 0.125) [45], and in $\text{La}_{1-x}\text{Ca}_x\text{MnO}_3$ ($x = 0.17$ and 0.2) [46]. But the importance of structural effects associated with the transition (variation of the orthorhombicity, superstructure peaks), calls for an investigation of the lattice excitations in both types of compounds, which has never been reported up to now in this doping range.

1.5. Outline

In the following, we focus on three compounds belonging to the F precursor phase, namely $\text{La}_{0.83}\text{Ca}_{0.17}\text{MnO}_3$, $\text{La}_{0.875}\text{Sr}_{0.125}\text{MnO}_3$ and $\text{La}_{0.8}\text{Ca}_{0.2}\text{MnO}_3$. In section 2, their transport, structural and magnetic properties will be examined. The observations resulting from inelastic neutron studies performed on these compounds will be reviewed and discussed in sections 3 and 4 for phonon modes and magnon modes respectively. A general discussion will be given in section 5.

Neutron scattering experiments have been carried out at the reactor Orphée (Laboratoire Léon Brillouin) and at the Institut Laue Langevin on triple-axis spectrometers using thermal and cold neutron sources. The samples are single crystals. $\text{La}_{0.83}\text{Ca}_{0.17}\text{MnO}_3$ and $\text{La}_{0.8}\text{Ca}_{0.2}\text{MnO}_3$ have been grown by Y M Mukovskii and D Shulyatev from the MISIS Institute in Moscow and $\text{La}_{0.875}\text{Sr}_{0.125}\text{MnO}_3$ by P Reutler from the Laboratoire de Physico-Chimie in Orsay, France. The wavevectors are defined as $\mathbf{Q} = \mathbf{q} + \boldsymbol{\tau}$. In this paper, only the Bragg peaks $\boldsymbol{\tau}$ are indexed within the orthorhombic structure. For magnetic and lattice excitations for which the perovskite cube is the most relevant, the wavevector \mathbf{q} values are indexed in the pseudo-cubic structure. All samples were twinned, so that, for instance, directions such as $[001]$, $[010]$ and $[100]$, in the pseudo-cubic notation, were superimposed. In the figures of this paper, where only one direction is specified, the other superimposed directions are termed ‘related symmetry directions’.

2. Transport, structural and magnetic properties

2.1. Resistivity

Figure 3 displays the temperature variations of the resistances or resistivity of the three compounds [23, 26]. For the compound $\text{La}_{0.875}\text{Sr}_{0.125}\text{MnO}_3$, this variation has already been reported by Pinsard *et al* [23]. For $x_{\text{Ca}} = 0.17$ (figure 3(a)) and $x_{\text{Ca}} = 0.20$ (figure 3(c)), the variation is very close to that reported by Okuda *et al* and Markovitch *et al* [24, 25]. Below $T_C = 175$ K ($x_{\text{Ca}} = 0.17$) or $T_C = 180$ K ($x_{\text{Ca}} = 0.20$), in a small temperature range, the variation presents a positive slope, characteristic of a ‘metallic’ or ‘quasi-metallic’ behaviour. Below 150 K, a smooth upturn indicates the occurrence of an insulating state. This variation shows strong similarities with that observed in $\text{La}_{0.875}\text{Sr}_{0.125}\text{MnO}_3$ [23] (figure 3(c)). However, in this latter case, the boundaries between the different regimes are much better defined. Three characteristic temperatures are determined: $T_{JT} = 280$ K, identified as the Jahn–Teller transition from the parameter variation of figure 4, $T_C = 178$ K where a ‘metallic’ behaviour occurs, identified as the Curie temperature from the magnetic Bragg peaks (figure 5) and $T_{O'O''} = 159$ K, where an insulating behaviour takes place.

2.2. Structural properties

Figure 4 reports the temperature dependence of the lattice parameters determined by neutron scattering in $\text{La}_{0.83}\text{Ca}_{0.17}\text{MnO}_3$ and by x-rays in $\text{La}_{0.875}\text{Sr}_{0.125}\text{MnO}_3$ previously reported by Pinsard *et al* [23].

The two compounds exhibit strong similarities. In the high-temperature range, the symmetry is pseudo-cubic and a single lattice parameter is determined. In $\text{La}_{0.83}\text{Ca}_{0.17}\text{MnO}_3$, where this determination has been obtained by neutron scattering, the structure becomes orthorhombic at $T_{JT} = 240$ K. Below $T \approx 150$ K, a decrease in the orthorhombicity is observed down to ≈ 75 K, where it remains constant. In this variation where the a and b parameters cannot be determined separately, the mean value of the $(a, b)_{eq}$ parameter decreases and the value of c increases so that the cell volume stays constant. In $\text{La}_{0.875}\text{Sr}_{0.125}\text{MnO}_3$, x-ray scattering measurements, with good enough resolution to separate a and b , yields a similar evolution for b and c between T_C and 130 K, whereas a is nearly constant. Moreover, Rietveld refinement, as reported by Pinsard *et al* [23] and Cox *et al* [35], reveals that the decrease in the orthorhombicity is concomitant with a variation of two of the three Mn–O distances. Their values, distinct in the intermediate ‘quasi-metallic phase’, become nearly equal below $T_{O'O''}$. In this variation, $T_{O'O''}$ corresponds to the inflection point. In $\text{La}_{0.8}\text{Ca}_{0.2}\text{MnO}_3$, the orthorhombicity which certainly exists, is too small to be detected within the q -resolution of the neutron scattering measurements. In figure 4(c), the temperature evolutions of the two superstructures, $(003)_{ortho}$ ($(0, 0, 2L + 1)$ type) and $(0\ 0\ 4.5)_{ortho}$ ($(0, 0, 2L + 1/2)$ type) determined by neutron scattering in $\text{La}_{0.875}\text{Sr}_{0.125}\text{MnO}_3$, are also reported. They appear at the same transition temperature $T = T_{O'O''}$. We emphasize that superstructures of the $(0, 0, 2L + 1)_{ortho}$ type are generally observed also in $\text{La}_{0.83}\text{Ca}_{0.17}\text{MnO}_3$ and $\text{La}_{0.8}\text{Ca}_{0.2}\text{MnO}_3$ but with strong irreversibilities, indicating metastability. In contrast, no superstructure of the $(0, 0, 2L + 1/2)_{ortho}$ type has been detected in either of the two Ca substituted compounds.

2.3. Magnetic Bragg peaks

Figure 5(a) displays the temperature dependence of the magnetic Bragg peak $(200)_{ortho}$, for $\text{La}_{0.83}\text{Ca}_{0.17}\text{MnO}_3$. Below a first anomaly of structural origin at T_{JT} , we observe an increase

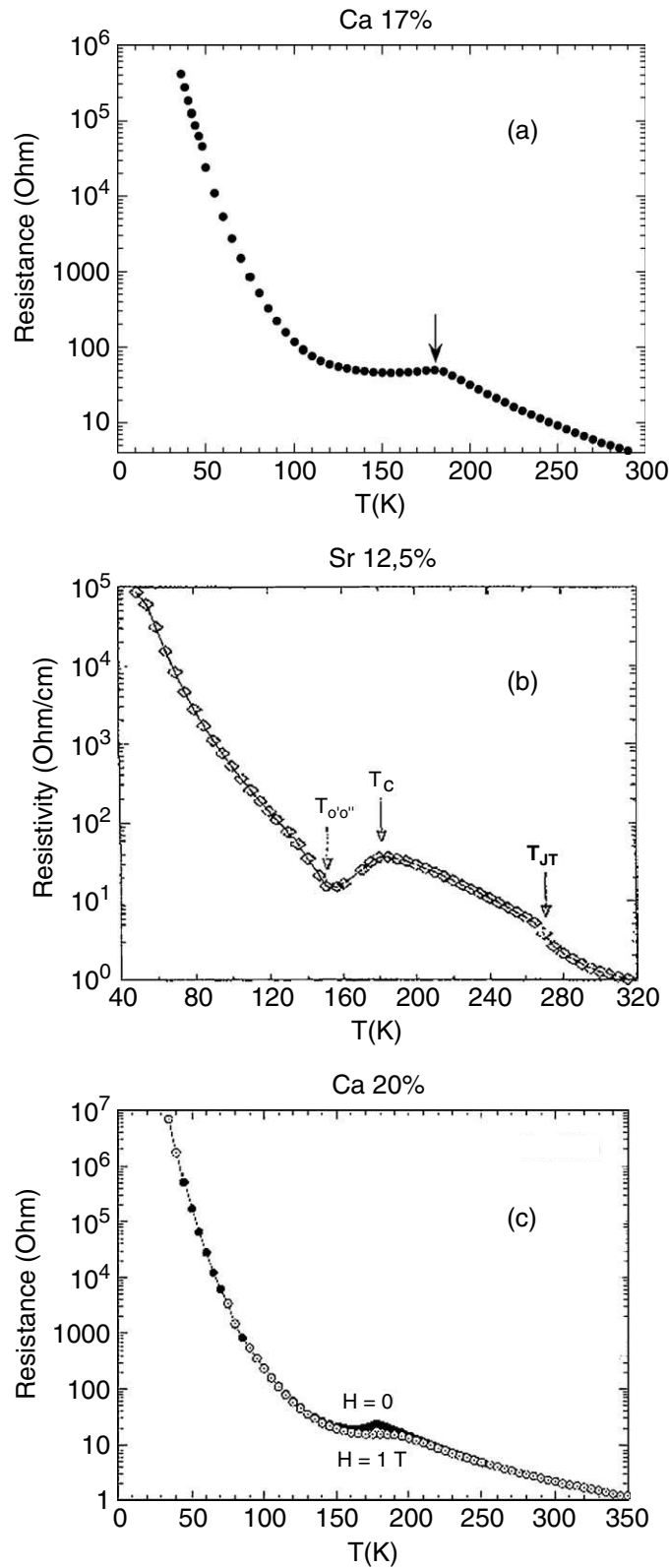


Figure 3. Temperature dependence of the resistance in $\text{La}_{0.83}\text{Ca}_{0.17}\text{MnO}_3$ (a) and $\text{La}_{0.8}\text{Ca}_{0.2}\text{MnO}_3$ (c). Temperature dependence of the resistivity in $\text{La}_{0.875}\text{Sr}_{0.125}\text{MnO}_3$ (b).

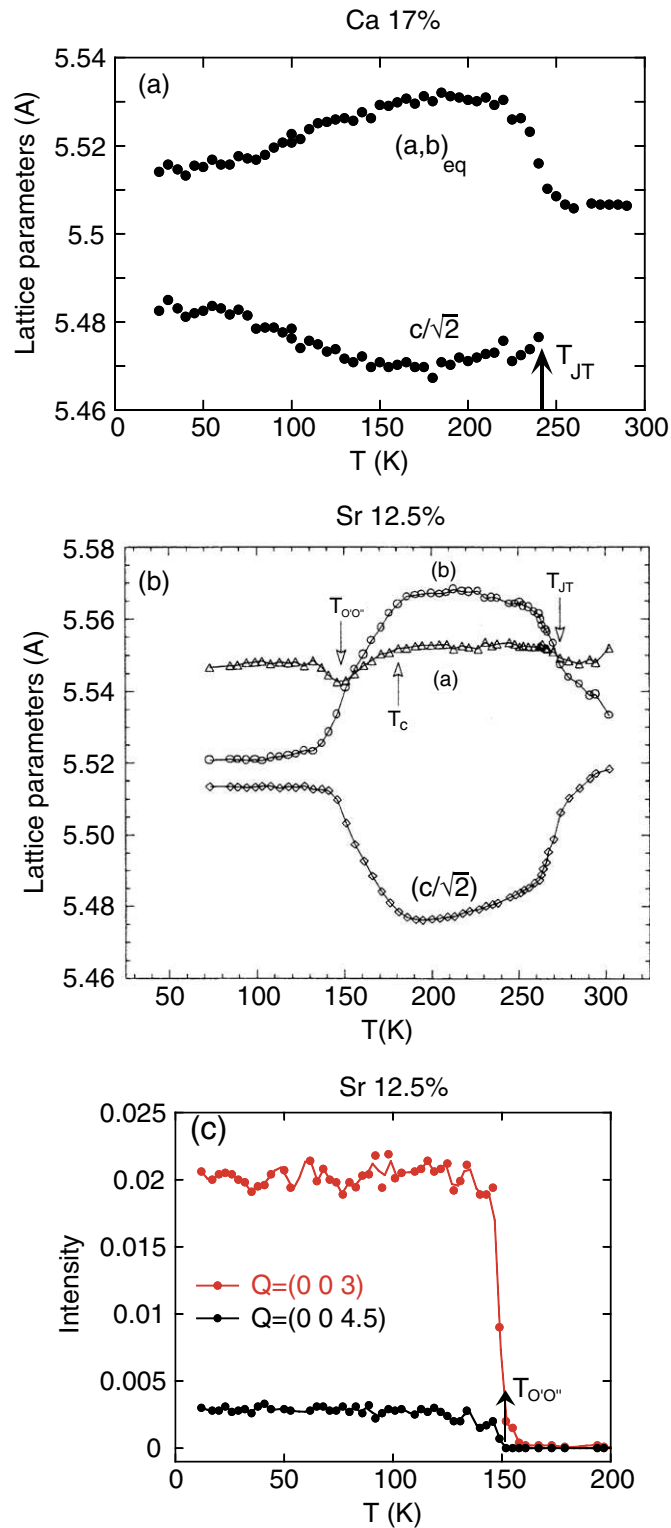


Figure 4. Temperature dependence of the lattice parameters in $\text{La}_{0.83}\text{Ca}_{0.17}\text{MnO}_3$ (a) and $\text{La}_{0.875}\text{Sr}_{0.125}\text{MnO}_3$ (b) in the orthorhombic structure. In (c), the temperature dependences of the superstructures $(0\ 0\ 3)_{ortho}$ and $(0\ 0\ 4.5)_{ortho}$ observed in $\text{La}_{0.875}\text{Sr}_{0.125}\text{MnO}_3$ are reported.

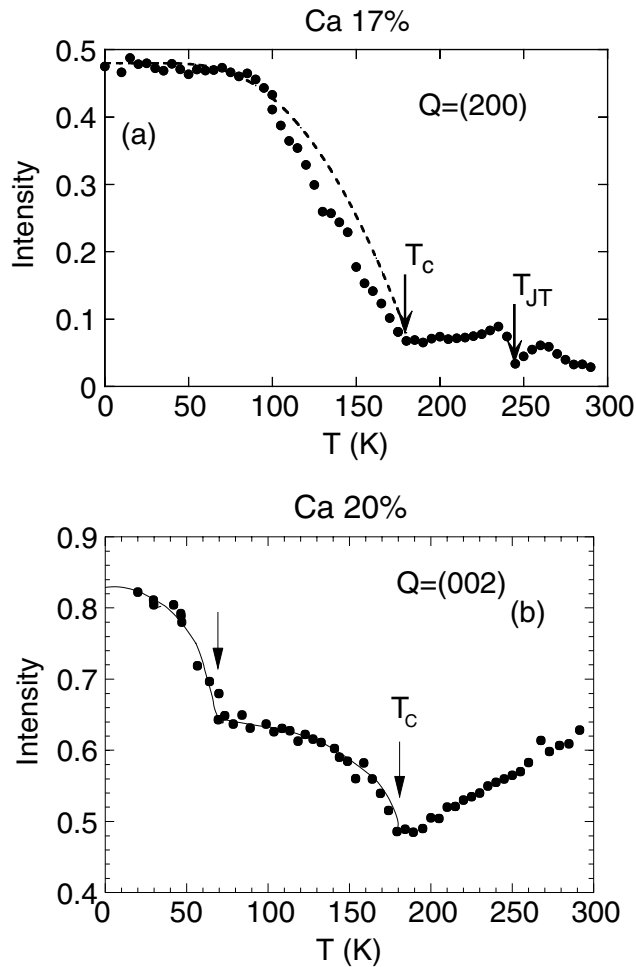


Figure 5. Temperature dependence of the $(200)_{ortho}$ Bragg peak in $\text{La}_{0.83}\text{Ca}_{0.17}\text{MnO}_3$ (a) and of the $(002)_{ortho}$ Bragg peak in $\text{La}_{0.8}\text{Ca}_{0.2}\text{MnO}_3$ (b). In (c), the intensities of the $(200)_{ortho}$ Bragg peak measured in zero-field (black circles) and in applied field (red circles) in $\text{La}_{0.8}\text{Ca}_{0.2}\text{MnO}_3$ are compared, at $T = 150$ K.

in the long-range F correlations determining $T_C = 175$ K. This temperature dependence with a linear part below T_C , suggests that, in the intermediate quasi-metallic phase, the F correlations do not develop as in a genuine ferromagnet. In figure 4(b), the variation of the $(002)_{ortho}$ Bragg peak in $\text{La}_{0.8}\text{Ca}_{0.2}\text{MnO}_3$ is also reported. An anomalous intensity increase is observed at 75 K (note that the scale of intensity in figure 5 does not start at zero). We stress that this anomaly is not systematically observed, but likely depends on the rate of cooling. In the case of $\text{La}_{0.875}\text{Sr}_{0.125}\text{MnO}_3$, magnetization measurements indicate a jump in the magnetization at $T_{O'O''}$. The temperature dependences of the magnetic Bragg peaks as well as that of the diffuse scattering between Bragg peaks, are actually very close to those previously reported by Kawano [30]. All these experiments emphasize the anomalous character of the intermediate F phase, with structural and magnetic disorder.

3. Phonon dispersion curves

3.1. $\text{La}_{0.8}\text{Ca}_{0.2}\text{MnO}_3$ and $\text{La}_{0.83}\text{Ca}_{0.17}\text{MnO}_3$

Let us recall that, for lattice and spin dynamics, wavevectors are indexed using cubic notations. The dispersions of transverse (TA) and longitudinal (LA) acoustic phonons, as well as the first and second optical phonon branches (LO) have been determined along the main symmetry directions for $\text{La}_{0.8}\text{Ca}_{0.2}\text{MnO}_3$ and are reported in figure 6(a)–(d). In addition, the TA branch along $[001]$, measured in $\text{La}_{0.83}\text{Ca}_{0.17}\text{MnO}_3$, is displayed in figure 6(e)–(g).

In $\text{La}_{0.8}\text{Ca}_{0.2}\text{MnO}_3$, the phonon dispersion curves are close to those previously determined in $\text{La}_{0.7}\text{Sr}_{0.3}\text{MnO}_3$ by Reichardt and Braden [49]. The new feature appears along $[001]$ where the TA acoustic phonon is very sensitive to the structural changes which occur in this concentration range. In the temperature range where the structural $(003)_{ortho} = (00\frac{3}{2})_{cub}$ superstructures are observed ($T \leq T_C$), this branch appears folded with respect to $q = 0.25$, which becomes a new zone boundary. No significant damping of this phonon branch is observed. This ‘classical’ effect, is illustrated in figure 6(b) at $T = 145$ K, where a new TA’ branch appears because of the folding. As expected, this folding effect exhibits irreversibility or metastability as observed for the $(003)_{ortho}$ peak.

In figure 6(e), the dispersion of the TA branch of $\text{La}_{0.83}\text{Ca}_{0.17}\text{MnO}_3$ at 150 K is reported. At this concentration, where a magneto-structural transition is observed below 150 K, two interesting features can be mentioned. Firstly, a softening of the TA branch is observed below 150 K as illustrated in figure 6(f). The amplitude of this softening, which is $\approx 15\%$ for $q = 0.1$, decreases with increasing q . This variation has to be related to the anomalous variation of the lattice parameters (figure 4(a)) which characterizes the magneto-structural transition. A similar effect, not illustrated here, has been observed in $\text{La}_{0.875}\text{Sr}_{0.125}\text{MnO}_3$, with a larger amplitude ($\approx 30\%$ at $q = 0.1$). The second interesting feature concerns the q -dependence of the damping of the TA phonons. As shown in figure 6(g), an anomalous increase of this damping appears at $q = 0.25$ below T_C . This could indicate a tendency for the TA dispersion curve to fold at this q value, as observed in $\text{La}_{0.8}\text{Ca}_{0.2}\text{MnO}_3$ (figure 6(b)). One cannot exclude an interaction with the magnon of the same q , which lies at a close energy value (≈ 10 meV). No such effects have been found for the LA phonon branch.

3.2. $\text{La}_{0.875}\text{Sr}_{0.125}\text{MnO}_3$

In figure 7, we have reported the dispersions of the TA, LA and LO phonon modes determined in $\text{La}_{0.875}\text{Sr}_{0.125}\text{MnO}_3$ along the $[001]$ direction at $T = 15$ K and along the $[110]$ direction at $T = 300$ K. Surprisingly, in this compound where superstructures are systematically observed below $T_{O'O'}$, no folding or anomalous damping of the TA branch is observed at $q = 0.25$. Only a slight softening anomaly can be seen, reported below in figure 13, where it is compared with the magnon energy. At smaller q , a stronger softening is found, similar to the $\text{La}_{0.83}\text{Sr}_{0.17}\text{MnO}_3$ case, as indicated above.

4. Spin-wave excitations

We focus on the $[100]$ and related symmetry directions, superimposed, except for $\text{La}_{0.8}\text{Ca}_{0.2}\text{MnO}_3$, where several directions are reported. Along the $[100]$ direction, the spin-wave

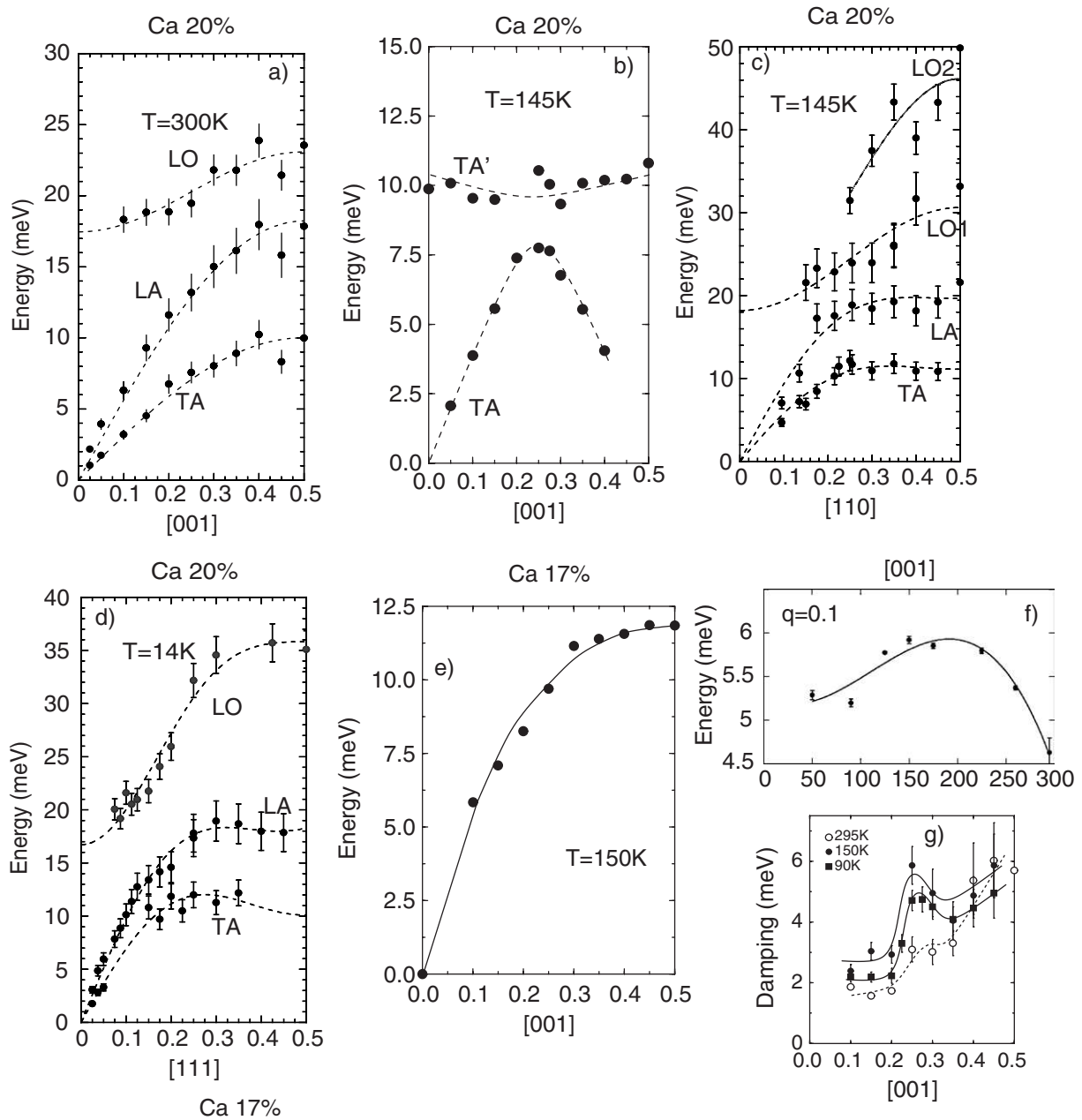


Figure 6. Phonon dispersions of the TA, LA, first and second LO branches in $\text{La}_{0.8}\text{Ca}_{0.2}\text{MnO}_3$ (a) along $[001]$ at $T = 300\text{ K}$, (c) along $[110]$ at $T = 145\text{ K}$, (d) along $[111]$ at $T = 14\text{ K}$. (b) Dispersions of the TA and TA' branches in $\text{La}_{0.8}\text{Ca}_{0.2}\text{MnO}_3$ along $[001]$ at $T = 145\text{ K}$. TA phonon branch along $[001]$ in $\text{La}_{0.83}\text{Ca}_{0.17}\text{MnO}_3$ for (e) dispersion at $T = 150\text{ K}$, (f) temperature dependence of the energy of the $q = 0.1$ mode, and (g) q -dependence of the TA phonon damping at 295 K (\circ), 150 K (\blacksquare) and 90 K (\bullet).

measurements have been performed in the second Brillouin zone, corresponding to the smallest \mathbf{Q} value for the energy range of interest. This allows us to keep the largest possible magnetic form factor and thus to get maximum magnetic neutron scattering cross-section. Furthermore,

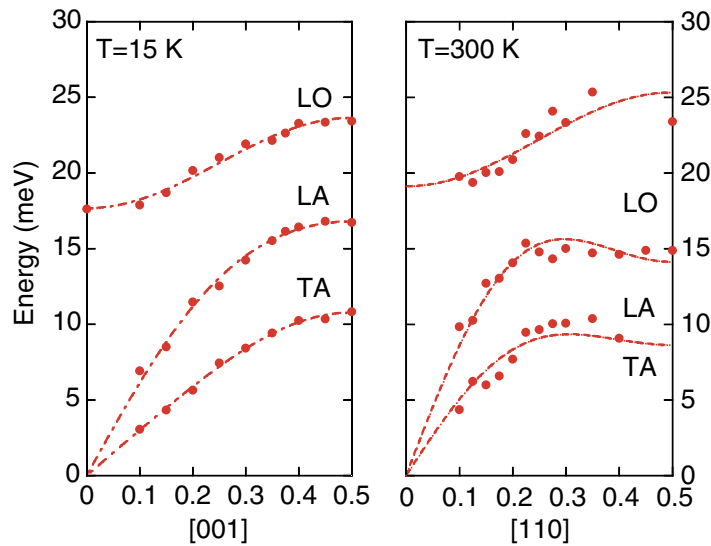


Figure 7. Dispersion of the TA, LA and LO phonon branches in $\text{La}_{0.875}\text{Sr}_{0.125}\text{MnO}_3$, along $[001]$ at $T = 15$ K (left panel) and along $[110]$ at $T = 300$ K (right panel).

we know from previous measurements that the phonon branches lying in this energy range have no sizable intensity in this Brillouin zone (except in some experiments which will be emphasized below).

Inelastic spectra have been fitted by a Lorentzian lineshape convoluted with the resolution function of the spectrometer. The energy E , damping Γ and intensity corrected from the Bose factor, are determined for each mode. The Bose factor is expected for propagative spin-waves. We emphasize that the damping value Γ is rather small ($E/\Gamma \approx 5$), and not significantly different from the damping of the magnetic excitations determined in the CAF state, previously reported [20]. Examples of fitted energy spectra are displayed for $\text{La}_{0.83}\text{Ca}_{0.17}\text{MnO}_3$ and $\text{La}_{0.875}\text{Ca}_{0.125}\text{MnO}_3$. In the case of $\text{La}_{0.8}\text{Ca}_{0.2}\text{MnO}_3$, examples of fitted spectra have been reported elsewhere [46].

4.1. $\text{La}_{0.83}\text{Ca}_{0.17}\text{MnO}_3$

4.1.1. Spin-waves along $[100] + [010] + [001]$. Figure 8 reports the $[001]$ direction and related symmetry directions. Measurements along $[110]$ and $[111]$ directions were also performed and will be reported elsewhere [50].

The spin-wave excitations are described by decreasing temperature from the quasi-metallic ($T = 150$ K) to the insulating ($T < 150$ K) state.

In figure 8, upper panel, the spin-wave dispersion curves determined at 150 K and 100 K along the $[001] + [100] + [010]$ directions are reported.

In the quasi-metallic state, at 150 K, a set of two branches labelled $(1 + 1')$ and (3) is clearly reminiscent of the two branches obtained in $\text{La}_{0.875}\text{Ca}_{0.125}\text{MnO}_3$ [20], at $T = 15$ K, as described in section 1 (cf figure 2, left and right parts of the lower panel). At this doping value $x_{\text{Ca}} = 0.125$, the large orthorhombicity makes it possible to assign the two branches to the two distinct **a** (or **b**) and **c** directions, which are superimposed because of twinning. This comparison allows us

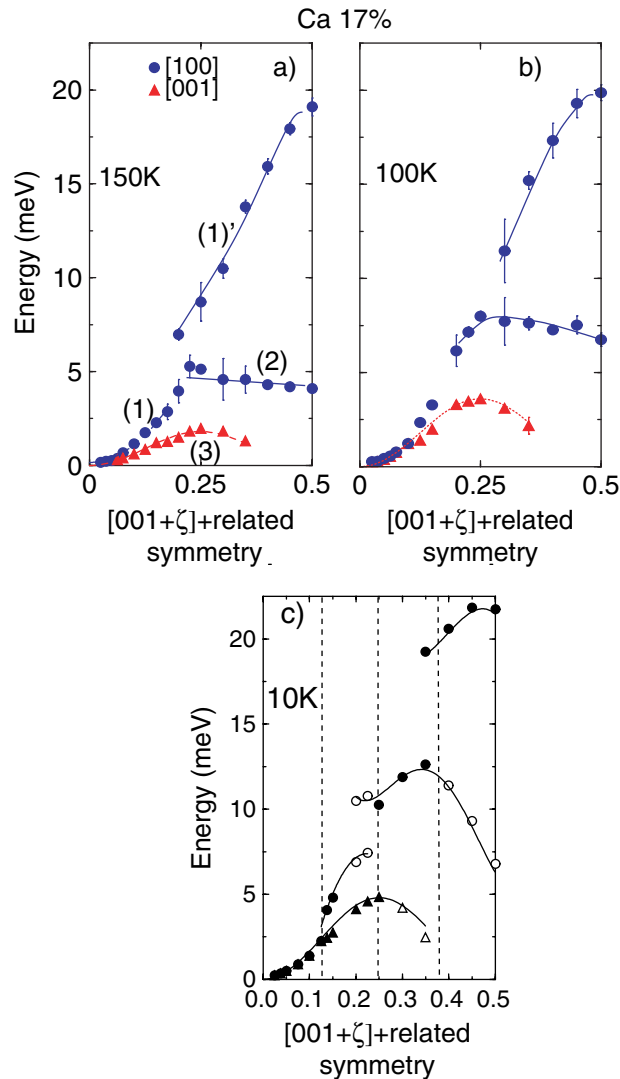


Figure 8. Dispersion of the magnetic excitations along $[001] + [100] + [010]$ at 150 K (a), 100 K (b) and 10 K (c) in a first zero-field experiment. The continuous curves are guides for the eye. In (c), the dashed vertical lines suggest underlying new zone boundaries.

to assign the curve (1 + 1'), dispersing up to 18 meV, to the $[100]$ (a) or $[010]$ (b) directions which are equivalent as far as magnetic coupling is concerned, and the curve (3) to the $[001]$ (c) direction.

Using this assignment, the two directions **a** (or **b**) and **c** can be described separately. In the small q -range ($q < 0.125$), the dispersion at $T = 150$ K is quadratic and very anisotropic, indicating a F coupling much stronger along **a** (or **b**) than along **c**, as observed in $\text{La}_{0.875}\text{Ca}_{0.125}\text{MnO}_3$ at 15 K.

At larger q , along **a** (or **b**), the new feature with respect to $x_{\text{Ca}} = 0.125$ is the gap opening in the dispersive curve (1). Within this gap, a nearly q -independent energy level exists, (2), at a mean value of 4.5 meV. Along **c**, the branch (3) exhibits the same down-turn around $q = 0.25$ as observed at $x_{\text{Ca}} = 0.125$ or in the CAF state when considering the SG branch [19, 20]

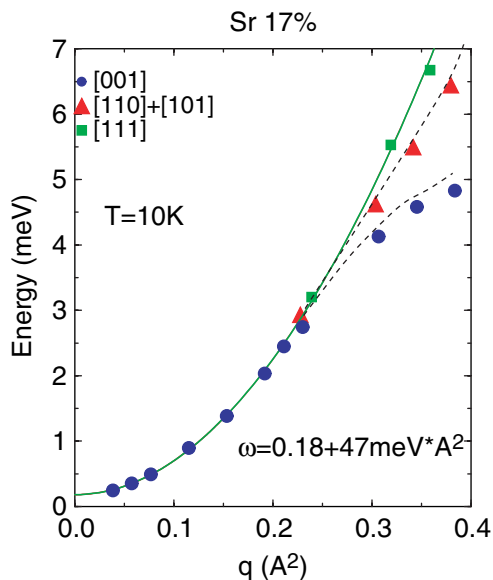


Figure 9. Spin-wave energy as a function of q in \AA^{-1} reported along the three symmetry directions. The experimental points attributed to the $[1\ 0\ 0]$ direction which depart from the common curve at and beyond $q \geq 0.125$ ($0.2\ \text{\AA}^{-1}$) have been omitted.

(figure 2, upper panel). In the CAF state, this down-turn is associated with a periodicity $2a$, characteristic of the AF ordering induced by the orbital ordering of LaMnO_3 . This persisting effect of the orbital-ordering along c in the $F\ \text{La}_{0.83}\text{Ca}_{0.17}\text{MnO}_3$ is very puzzling and cannot be understood in terms of an homogeneous magnetic state.

Upon decreasing temperature, from 150 K to 100 K, in the small q -range ($q < 0.125$), the weak dispersion observed along c rapidly stiffens to reach the dispersion value measured along a or b , so that at 100 K and below, the dispersion is isotropic. This isotropy is shown at 10 K in figure 9 where the dispersion curves are reported along three symmetry directions as a function of q in \AA^{-1} , yielding $D = 47\ \text{meV}\text{\AA}^2$.

Concomitantly with this evolution, we observe the onset of a q -dependence in the level labelled (2). Below 100 K, the modulation of this level is enhanced, defining a maximum in energy at $q \approx 0.35$. Larger gaps appear at $q \approx 1/4$ and $\approx 3/8$ and a new one opens at $q = 1/8$. This is illustrated in figure 8(c) at $T = 10\ \text{K}$. The changes in the dispersion are accompanied by a redistribution of the intensity of the modes. In figure 10, two energy spectra obtained at $q = 0.4$ for 125 K and 10 K are compared. The intensity of level (2) gradually decreases whereas that of the high-energy level increases, which is the opposite effect expected due to the thermal Bose factor. Therefore, below 100 K, the main intensity line looks like the dispersion of a split F branch.

4.1.2. Interpretation: confined spin-waves in two-dimensional F domains and charge ordering. Let us first discuss the quasi-metallic state and then the low-temperature insulating state.

In the quasi-metallic state, the quite new feature in the magnetic excitations with respect to $x_{\text{Ca}} = 0.125$ is the q -independent level observed at low energy ($\approx 4.5\ \text{meV}$ at 150 K). A q -independent energy level denotes a localized excitation. The existence of a gap-opening at the

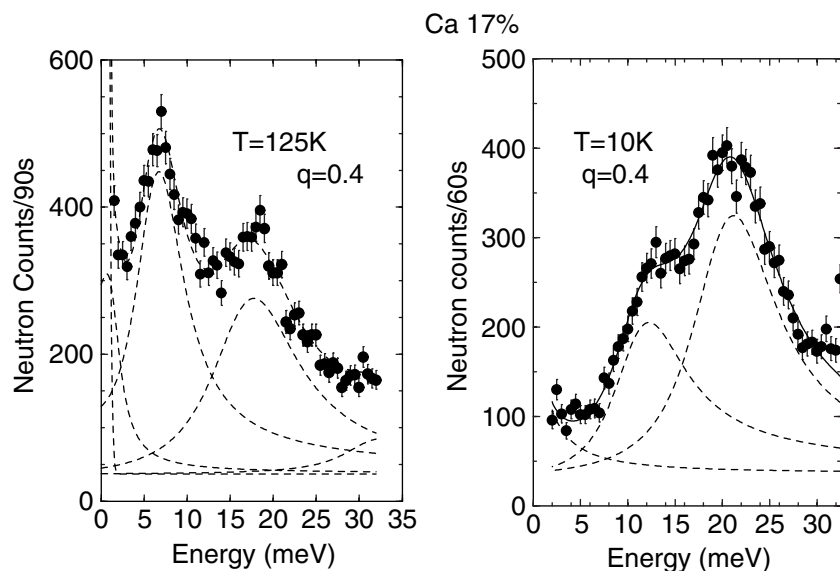


Figure 10. Comparison between two energy spectra at the same q ($q = 0.4$ in reduced lattice units) along $[100] + [010] + [001]$ and two temperatures, $T = 125$ K (left panel) and $T = 10$ K (right panel).

crossing of branches (1) and (2) indicates an interaction between this mode and the dispersive excitation. This implies that both excitations take place in the same macroscopic domain and also assigns the dispersionless branch to the **a** or **b** direction. In contrast, no anomaly is found along **c** where the spin-wave branch is very similar to that determined at lower concentrations. These overall observations emphasize the two-dimensional character of the localized excitations, confined in the (**a**, **b**) plane. This is confirmed by the observations of dispersionless branches also along the $[110]$ direction [50].

On the other hand, we notice that these excitations are only observed for q values larger than that of the crossing point. A first estimate of the domain size can be obtained as follows.

In the **a** or **b** direction, for wavelength values larger than the typical size of the domain (small q), only propagating excitations may exist. For wavelengths less than the typical size of the domain, both types of excitations, localized and propagating, exist and share the total intensity. The crossing point, q_{cr} , revealed by the gap-opening, can be related, qualitatively, to the domain size ξ . With $q_{cr} \approx 0.2$, this yields $\xi = a_0/q_{cr} \approx 20$ Å. We can even go one step further in the quantitative estimation, by considering the energy value of the q -independent level instead of the crossing value q_{cr} . This will be done below together with the discussion about the case $x_{Ca} = 0.2$.

In the insulating state, below 100 K, the above description is no longer valid as the q -independent level becomes modulated and new gaps open in the dispersion. A common explanation for the origin of gaps at $q = 1/8$, $1/4$ and $3/8$, as well as of the modulation around $3/8$, consists in assuming an underlying periodicity of $4a_0$ (and possibly, in addition, of $2a_0$) along **a** and **b**. Indeed, in that case, new zone boundaries corresponding to the super-cell exist, indicated by vertical dashed lines in figure 8(c), and the dispersive branch is folded at these positions, with new gap-openings. We emphasize that the absence of symmetry of level (2), on both sides of $q = 3/8$, cannot be explained with the only assumption of a first-neighbour coupling.

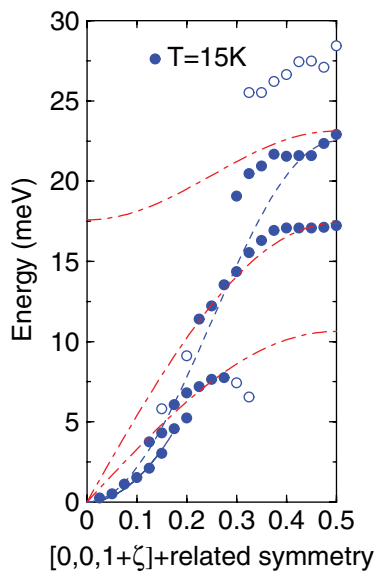


Figure 11. Magnetic excitations along $[001]$, with main (\bullet) and weak (\circ) intensity. The dot-dashed lines are fits of the phonon dispersion branches. The dashed line is a cosine law drawn by considering the magnetic modes with the dominant intensity.

Therefore, we can conclude that a charge-ordered state develops at low temperature, which, unlike the $\text{La}_{0.875}\text{Sr}_{0.125}\text{MnO}_3$ case, is not revealed by superstructure peaks, but through the magnetic excitations. The fact that the doping concentration ($x_{\text{Ca}} = 0.17$) is much larger than the stoichiometric $x = 1/8$ value where a charge-ordered state can be expected, could indicate that some holes are pinned on the lattice, causing a decrease of the effective hole doping value which contributes to the charge ordering transition. Such pinned holes could be related to the existence of short-range structural distortions, or correlated polarons, reported in this compound [40].

4.2. $\text{La}_{0.875}\text{Sr}_{0.125}\text{MnO}_3$

A previous spin-dynamics study at a slightly smaller concentration, $\text{La}_{0.91}\text{Sr}_{0.09}\text{MnO}_3$, corresponding to the CAF state, has shown the existence of two spin-wave branches as in Ca-doped compounds [19, 45]. The coupling constant along \mathbf{c} , deduced from the high-energy branch is negative (AF) and very weak, indicating the proximity of the F state ($J_c \approx 0$), which occurs at $x_{\text{Sr}} = 0.1$.

In absence of a complete study of the quasi-metallic state, we first describe the magnetic excitations in the low temperature insulating state ($T = 15$ K), then, the temperature dependence of the two specific magnetic modes at $q = 0.5$ and $q = 0.25$.

4.2.1. Spin-waves along $[100] + [010] + [001]$ at $T = 15$ K. The spin-wave dispersion curve obtained at $T = 15$ K is reported in figure 11, with the phonon dispersion curves, shown as dot-dashed lines (cf figure 7, left panel).

In the very small q -range, one dispersion curve is observed, obeying a quadratic law in agreement with a F state. Therefore, as in the compound $\text{La}_{0.83}\text{Ca}_{0.17}\text{MnO}_3$, the dispersion in the small q -range at low temperature, is mainly isotropic. This is confirmed by the study along $[110]$ [45].

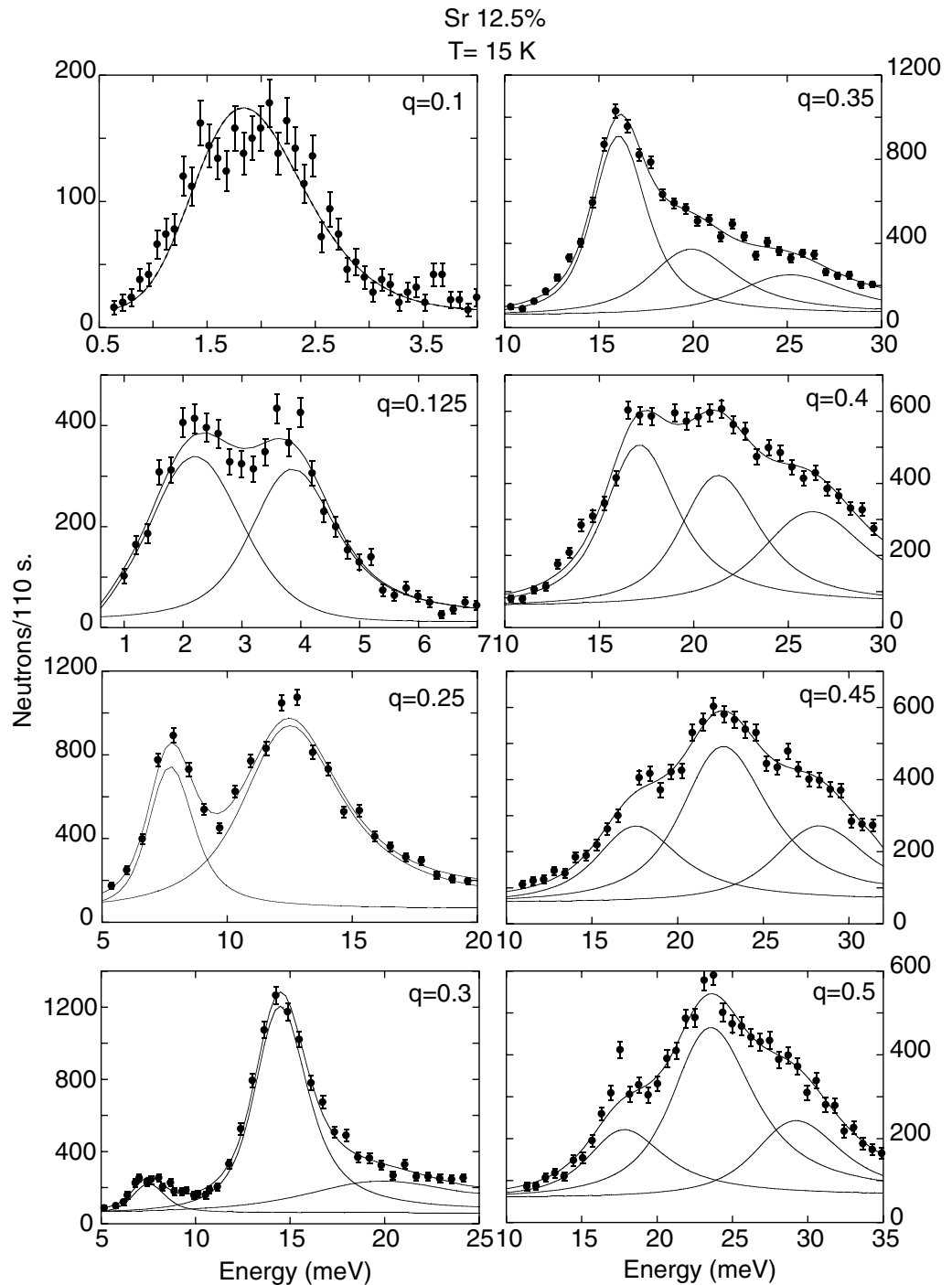


Figure 12. Energy spectra showing magnetic modes at several q values, from $q = 0.1$ to $q = 0.5$ along $[1\ 0\ 0]$ in $\text{La}_{0.875}\text{Sr}_{0.125}\text{MnO}_3$.

At $q \approx 0.125 = 1/8$, a small gap appears, defining a new mode at a higher energy. Then at larger q , other gaps appear in the dispersion, so that the overall dispersion curve is split into several branches. In any case, the magnon energy with dominant intensity obeys a cosine law (dashed line in figure 11), as expected in a F state. Some raw data are displayed in figure 12 which illustrate this q dependence.

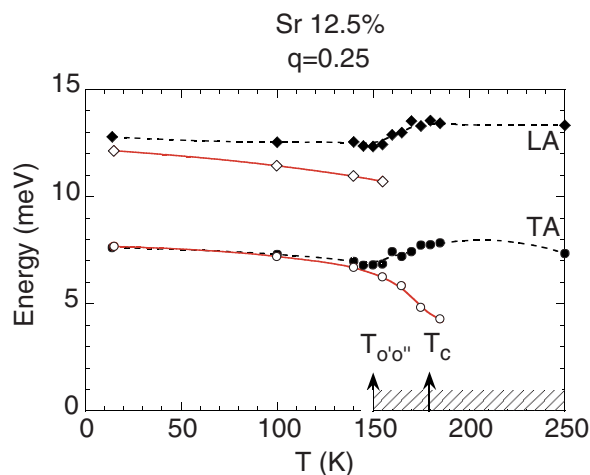


Figure 13. Temperature dependences of the magnetic excitations (red circles) and of the TA and LA phonon modes (black circles) at $q = 0.25$ along $[100]$. The hatched area corresponds to a quasi-elastic signal.

Furthermore, a striking coincidence is observed in a wide energy range, between the positions of the magnon branches and those of the phonon ones. As seen in figure 11, magnon modes are found at energies corresponding to the TA phonon branch at small q values, then at energies corresponding to the LA branch at intermediate q values and finally at energies corresponding to the LO branch, close to the zone boundary.

The magnetic origin of these branches is deduced from their temperature dependence. The temperature dependence also indicates that the coincidence between magnon and phonon energies observed at 15 K is probably not fortuitous, suggesting a peculiar magnon–phonon coupling. The magnetic modes with wave-vectors $q = 0.25$ and 0.5 have been specifically studied. These two wavevectors correspond precisely to the static superstructure peaks which grow below $T_{O'O''}$.

In a previous paper [45], we have reported the temperature evolution of the magnetic excitations at $q = 0.5$. At this q value, in the quasi-metallic state ($T = 160$ K), three modes are clearly identified, respectively at the energy of the TA, LA and LO phonon modes. In addition, a quasi-elastic intensity is observed. As temperature decreases, these three modes shift towards the energy of the LA (17 meV) and LO (23 meV) phonon modes for two of them and towards a higher energy value (28 meV) for the third one, as shown in figure 11 at 15 K, whereas the quasi-elastic intensity disappears.

The temperature evolution of the excitations at $q = 0.25$, illustrated in figure 13, is especially interesting since it suggests that this mode could play some role at the transition. In this figure, both magnetic modes (\circ) and phonon modes (\bullet) have been plotted. At high temperatures, in the ‘quasi-metallic’ state, a single magnetic mode is mainly observed with a low energy (≈ 3 meV), distinct from zero even at T_C . In addition, a quasi-elastic mode is determined, which actually exists in the whole q -range [45]. It is indicated by the hatched area in figure 13. At the transition $T_{O'O''}$, below which superstructure peaks appear, the inelastic mode matches the TA phonon energy value, then follows its temperature dependence down to 14 K, the lowest temperature studied. Concomitantly, the quasi-elastic mode disappears and an intensity transfer is observed from the magnetic mode lying at the ‘TA’ energy to that lying close to the ‘LA’ energy. The

latter mode is too weak above $T_{O'O''}$ to be ascertained, but becomes clearly observable below this temperature.

In order to further check the nature of these excitations, experiments with polarized neutrons and polarization analysis have been also performed at this value of $q = 0.25$, in the same Brillouin zone. They confirm the transverse character of these magnetic excitations, as expected for usual spin-waves, but fail to detect any phononic contribution.

4.2.2. Discussion. The study of the spin-wave spectrum in $\text{La}_{0.875}\text{Sr}_{0.125}\text{MnO}_3$ has revealed features, some of which are common to $\text{La}_{0.83}\text{Ca}_{0.17}\text{MnO}_3$, but others distinct. The existence of several magnetic branches, both in the intermediate ‘metallic’ and in the insulating states appears to be a common feature of this F state (cf section 2 for $x_{\text{Ca}} = 0.17$ and section 4 for $x_{\text{Ca}} = 0.2$). Also, the temperature evolution of these magnetic excitations, with a transfer of spectral weight from the lower energy level in the metallic state to the higher energy level in the insulating state, is very similar in both compounds. We note that this evolution of the intensity is opposite to that expected from the thermal Bose factor. Therefore, the magnetic excitations in $\text{La}_{0.875}\text{Sr}_{0.125}\text{MnO}_3$ and $\text{La}_{0.83}\text{Ca}_{0.17}\text{MnO}_3$ exhibit very similar features. In the case of $\text{La}_{0.83}\text{Ca}_{0.17}\text{MnO}_3$, where the magnetic excitations have been determined in the whole q -range in the quasi-metallic state, the weakly dispersed level could be attributed to a confined spin-wave inside F clusters lying within the (**a**, **b**) plane. A similar picture could exist for $\text{La}_{0.875}\text{Sr}_{0.125}\text{MnO}_3$. This will be discussed elsewhere in connection with the general study of the quasi-metallic state.

The other prominent feature of the Sr-doped compound is the observation of a coincidence between phonon and magnon energies. This is clearly observed along $[001]$ at $q = 0.5$ in the whole temperature range. Such a coincidence seems to play a specific role in the transition at $q = 0.25$, where the magnetic mode matches the TA phonon mode, precisely at and below $T_{O'O''}$. At low temperature, this coincidence between magnon and phonon modes is observed in a wide q -range. These observations strongly suggest the existence of a peculiar magnon–phonon coupling, although direct evidence for such a coupling using polarized neutrons has not yet been obtained. In this compound where superstructure peaks are systematically observed below $T_{O'O''}$ at $q = 0.25$ and 0.5 , we could expect a folding of the magnetic dispersion curve, characteristic of these new periodicities, as found in $\text{La}_{0.83}\text{Ca}_{0.17}\text{MnO}_3$. In agreement with this expectation, a small gap is observed at $q = 1/8$. However, the folding of the dispersion curve at $q = 1/4$ and $3/8$ is not seen, likely overcome by this magnon–phonon coupling.

Magnetic excitations coupled with charge ordering and phonons could constitute a new type of excitations specific to this low-temperature ground state. Such a coupling between charge–spin–lattice degrees of freedom could assist the structural transition, giving rise to lattice superstructures at $q = 0.25$ and 0.5 and possibly explain the first-order character of the transition. This interpretation is supported by theoretical work [52] which outlined the role of long-range elastic interactions in stabilizing a charge-ordered state.

4.3. $\text{La}_{0.8}\text{Ca}_{0.2}\text{MnO}_3$

The study of $\text{La}_{0.8}\text{Ca}_{0.2}\text{MnO}_3$ mainly concerns the intermediate ‘quasi-metallic’ state at $T = 150$ K. Comparing the results with observations made in $\text{La}_{0.83}\text{Ca}_{0.17}\text{MnO}_3$, reveals a very interesting evolution with x . Preliminary experiments performed at low temperature and along one direction have previously been reported [20].

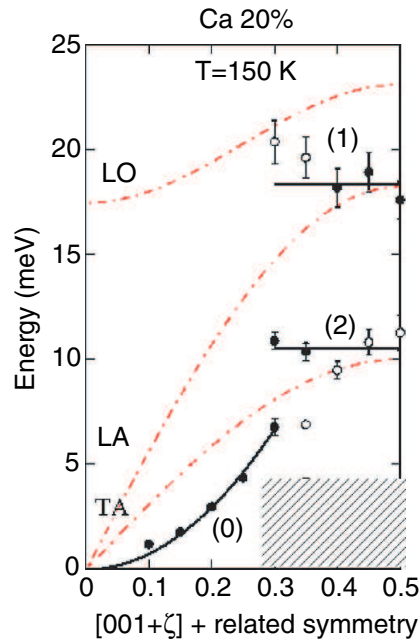


Figure 14. (a) Spin-wave dispersion along $[001]$ at $T = 150$ K in a first zero-field experiment. Dot-dashed lines are fits of the phonon dispersion curves reported in figure 5. The small- q dispersion curve is labelled (0) and the two q -independent levels are labelled (1) and (2). The hatched area corresponds to quasi-elastic modes.

4.3.1. Spin-waves along $[100] + [010] + [001]$. First $H = 0$ experiment: in figure 14, the magnetic excitations measured in the ‘quasi-metallic’ state, in a first zero-field experiment are reported. In addition, the phonon branches lying in this energy range are shown by dot-dashed lines. At 150 K, a single spin-wave dispersion branch labelled (0) is observed up to $q \approx 0.25$ – 0.3 . This indicates that the $[100]$ or $[010]$ (equivalent) directions, are identical to $[001]$ (c direction). Therefore, unlike the $x_{\text{Ca}} = 0.17$ case, the dispersion is isotropic even in the ‘metallic’ phase. This isotropy is confirmed by experiments along the other directions leading to a stiffness constant $D = 30 \text{ meV } \text{\AA}^2$ (as compared to $47 \text{ meV } \text{\AA}^2$ determined at 14 K, the same value as in $\text{La}_{0.83}\text{Ca}_{0.17}\text{MnO}_3$). Beyond this q value, the magnetic intensity is distributed between three nearly q -independent modes, defined by their mean values: a high-energy mode (1) around 18 meV, an intermediate mode around 10 meV (labelled (2)) and a quasi-elastic mode or overdamped mode at low energy (hatched area in figure 14). We note that the energies at the zone boundary ($q = 0.5$) coincide with those of the TA and LA phonon branches, suggesting that these phonons may play some role in stabilizing these q -independent magnetic levels.

$H = 0$ experiment, after field application: a magnetic field ($H = 2$ T) applied at 150 K suppresses the quasi-elastic scattering attributed to the spin fluctuations and reduces the damping of the nearly q -independent magnetic levels. Another level, labelled (3), likely mixed with the quasi-elastic peak in the first $H = 0$ experiment, now appears well-defined at ≈ 4.5 meV. When removing the field at 150 K, the spin fluctuations remain considerably reduced and the magnetic levels mainly retain the characteristics observed in the applied field. The magnetic excitations observed in zero field after field application, are shown in figure 15 (left panel). A slight dispersion

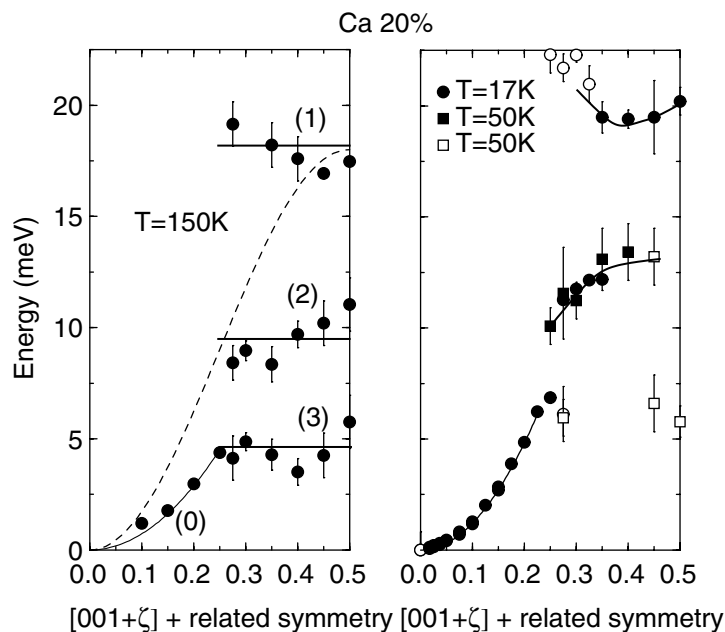


Figure 15. Spin-wave dispersion along $[001]$ in a zero-field experiment after applying a magnetic field, at 150 K (left panel) and 50 K and 17 K (right panel). The small- q dispersed branch is labelled (0) and the nearly dispersionless levels are numbered from (1) to (3). The dashed line is a cosine law corresponding to a F state. Continuous lines are guides for the eye.

in the level (2), absent in the first zero-field experiment (figure 14), can be seen. We also mention that the LO phonon mode, which was unobservable in the second Brillouin zone, in the first $H = 0$ experiment, is now observed at ≈ 24 meV, separated from the magnetic level (≈ 18 meV). A similar effect of the field on the intensity of the LO phonon mode has been also observed in the $x_{\text{Ca}} = 0.17$ compound.

As temperature increases up to T_C and above, the q -dispersed branch (0) defined in the first half Brillouin zone renormalizes to zero, as expected for a F state. In contrast, the q -independent energy levels observed in the larger- q range vary slowly. This further indicates that the magnetic couplings, probed either by the small- q branch or by the q -independent levels in the large- q range, have a distinct origin and that the F transition is driven by the coupling involved in the dispersive branch only. We recall that a similar conclusion has been reached in the CAF state where only the SG branch but not the LG one can be readily related to T_C , as shown in $\text{La}_{0.9}\text{Ca}_{0.1}\text{MnO}_3$ [20].

Upon decreasing the temperature in zero field, a transfer of spectral weight is observed from the lower to the higher levels whereas the small- q dispersion stiffens. Therefore the lower energy mode (3) nearly disappears and level (2) becomes more dispersed, which reduces the energy gap at $q = 0.25$ (figure 15, right panel). The overall magnetic spectrum corresponds to a split F dispersion curve.

4.3.2. Spin-waves along $[110]$ and $[111]$ at $T = 150$ K. Spin-wave measurements along $[110] + [101] + [011]$ and $[111]$ (for which all domains are equivalent) have also been measured at 150 K and 15 K. Figure 16 reports observations obtained in the quasi-metallic state

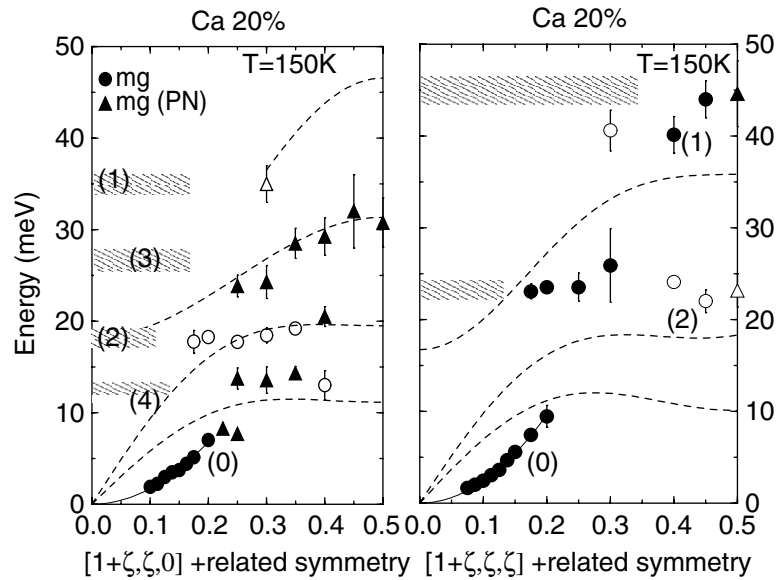


Figure 16. Magnetic excitations (mg) for q along $[1\ 1\ 0] + [0\ 1\ 1] + [1\ 0\ 1]$ (left panel) and along $[1\ 1\ 1]$ (right panel) at $T = 150\text{ K}$, measured with unpolarized (\circ) and half-polarized (\triangle) neutrons. Full (empty) symbols refer to modes with main (weak) intensity. The hatched area corresponds to calculated levels (see the text). Dashed lines are fits of the phonon branches measured at the same temperature.

(150 K) along the $[1\ 1\ 0]$ direction (left panel) and along the $[1\ 1\ 1]$ direction (right panel). Along the $[1\ 1\ 0]$ direction, which is superimposed on the $[1\ 0\ 1]$ or $[0\ 1\ 1]$ directions, the entanglements between magnon and phonon branches led us to use polarized neutrons, which allow us to separate magnons from phonons. Besides a small- q dispersive branch labelled (0), several levels of magnetic origin are observed, weakly dispersed. We note a coincidence between the magnetic modes and the LO branch around 25 meV, which could also suggest a peculiar magnon–phonon coupling. Using polarized neutrons, because of a poor intensity, no magnetic modes could be determined above 35 meV. Along $[1\ 1\ 1]$, beyond the small- q dispersive branch, two dispersionless energy levels are observed, one at $\approx 23\text{ meV}$ and one around 46 meV. With decreasing temperatures, the energy of the magnetic modes slightly increase ($\approx 12\%$ at 15 K), but the split character of the dispersion persists.

4.3.3. Discussion: confined spin-waves in 3D isotropic clusters. The main observation corresponds to the existence of discrete energy levels. They reveal local excitations inside coupled spin domains. The small damping value of the modes indicates that these domains are very similar.

Actually, these overall observations can be explained as follows. In contrast to $\text{La}_{0.83}\text{Ca}_{0.17}\text{MnO}_3$, where the q -independent levels are associated with q directions in the (\mathbf{a}, \mathbf{b}) plane only, the perfect isotropy of the small- q dispersion observed in the present case suggests that the q -independent levels exist along all directions. We propose to attribute them to spin-waves confined within 3D clusters. A model is clearly needed to assign each level to one specific direction, \mathbf{a} or \mathbf{c} for example, along $[0\ 0\ 1] + [1\ 0\ 0] + [0\ 1\ 0]$, and to determine a cluster size.

In a finite-size F cluster for which several modes are expected, each eigenvalue shows a continuous distribution of q , which becomes narrower as the size increases whereas the lowest energy level decreases. A model of magnetic excitations in F clusters has been proposed by Hendriksen *et al* [51] in which the coupling between the spins is described using a Heisenberg model with first nearest-neighbour couplings. This model is valid for isotropic clusters. The authors deduce from their calculations that, for small clusters, the eigenvalue with the lowest energy is a half wavelength or a half period of a standing wave, whereas it increases to a full wavelength for larger clusters. In the following, we assume that the first standing wave corresponds to a half period, considering that this assumption provides a lower limit for the size determination.

Based on this model, in a previous paper [46], we have used the expression of the energy of the propagative wave in a three-dimensional Heisenberg model with two distinct coupling values, $J_{a,b}$ and J_c corresponding to **a** or **b** and **c** directions respectively. $J_{a,b}$ and J_c are readily related to the energy values at the zone boundary E_B along the various directions. These relations should also be valid for finite-size clusters where the coupling constants characterize the spin interactions inside the cluster. In the present case, where E_B along [1 1 0] could not be determined, $J_{a,b}$ and J_c are obtained under some assumption by considering the [1 0 0] + [0 1 0] + [0 0 1] directions only and then the obtained values are used to determine the energy levels along all the other directions.

Along [1 0 0], the mode with the highest energy level E_B , should correspond to nearest-neighbour spins fluctuating in opposite phase, so that a half period corresponds to one lattice spacing. One expects therefore that the lowest energy level, which is assumed to correspond also to a half period, should be a sub-multiple of E_B . The size can be deduced from the ratio between the lowest energy level, and E_B .

In figure 15, level (1), which defines the energy of the first neighbour coupling, and level (2) at half this value are attributed respectively to the full and half waves confined inside a domain of two lattice spacings along [1 0 0] or [0 1 0]. Similarly, level (2) (≈ 9 meV) and level (3) at half this value (≈ 4.5 meV) are attributed to the full and half wave along the **c** or [0 0 1] direction. Level (2) corresponds therefore to two levels associated with two distinct directions [0 0 1] and [1 0 0]), which are superimposed because of twinning. Using the energy values of the high-energy level along each distinct direction ($E_B^{[100]} \approx 18$ meV and $E_B^{[001]} \approx 9$ meV), we determine $J_{a,b} = 1.12 \pm 0.1$ meV and $J_c = 0.56 \pm 0.05$ meV.

By assuming a cubic or a nearly spherical shape, we determine the two levels in all other symmetry directions by using the relations between the zone boundary energies. These levels are shown by hatched area instead of narrow lines in figure 17 because of limited experimental accuracy. The good agreement with experimental values supports this interpretation.

Let us come back now to the case of $\text{La}_{0.83}\text{Ca}_{0.17}\text{MnO}_3$. The energy values at the zone boundary, which is ≈ 19 meV along [1 0 0] reported here and ≈ 38 meV along [1 1 0] and ≈ 39 meV along [1 1 1], reported elsewhere [50], determine $J_{a,b} = 1.125$ meV and $J_c = 0.19$ meV. The very small value of J_c , likely explains the two-dimensional character of the confined spinwave reported in experiments along [1 0 0]. Along [0 0 1], the energy value of the q -independent level, ≈ 4.5 meV, is 1/4 of the energy value of the zone boundary. Although only one level is stabilized here (one could expect four levels), we consider that it corresponds to the lowest-energy level. It is attributed therefore to a confined wave with a half period. From the 1/4 ratio value, a spin domain consisting of four lattice spacings along **a** or along **b** is obtained. This determines a size of 16 Å, slightly smaller than our previous determination (cf section 4.1).

5. General discussion

In the quasi-metallic state, particularly studied in the two Ca-substituted compounds, the inelastic neutron scattering has revealed the existence of magnetic energy levels, typical of magnetic excitations in small F clusters. The temperature evolution of their intensity, which does not follow Bose statistics, recalls the evolution expected for magnetic quantum levels in superparamagnetic spin clusters [47]. These observations agree with the superparamagnetic behaviour observed by Mossbauer spectroscopy [43]. The existence of clusters or domains with a typical size, implies that the magnetic characteristics differ over the scale of the cluster and points out a charge segregation. The determination of anisotropic values for the magnetic coupling constants, with $J_{a,b}$ larger than J_c , reminds the orbital-ordered state of LaMnO_3 , and therefore suggests a ‘superexchange’ character. This suggestion is also supported by the variation of $J_{a,b}$ and J_c with doping recently reported [46], showing a monotonic increase of their absolute value, when going from the CAF state, where $J_{a,b,c}$ characterizes the Mn^{3+} matrix, towards the F state. We may conclude that the clusters are hole-poor. In contrast, the cluster boundaries may consist of hole-rich or metallic orbital-disordered state. If this picture is exact, it would mean that, because of some constraints, these mobile holes induce a weak F inter-cluster coupling, smaller than the ‘superexchange’ coupling determined inside the clusters.

Within this picture, the overall evolution with doping can be described as follows. In the CAF state, the magnetic inhomogeneities are hole-rich, strongly anisotropic (platelets within the **(a, b)** plane), with a little size variation from $\approx 16 \text{ \AA}$ to 20 \AA as x increases [53]. At $x_{cr} = 0.125$, they ‘percolate’. For $x > 0.125$, in the quasi-metallic state of the $x_{Ca} = 0.17$ sample, 2D orbital-ordered domains occur with $\xi \approx 16 \text{ \AA}$ surrounded by a ‘metallic’ orbital-disordered network. We outline that this orbital-disordered or metallic network preserves the long-range orbital ordering along **c**, as shown by the persisting anisotropy of the stiffness constant, and by the large orthorhombicity. We may suggest a picture of orbital-ordered tubes more or less distorted along **c**, the 2D spin domains corresponding to their transversal section within the **(a, b)** plane. Finally, in the last step, illustrated by the $x_{Ca} = 0.2$ sample, small orbital-ordered domains, isotropic, with $\xi \approx 8 \text{ \AA}$ occur. There, the orbital-ordering is broken in all directions on a nanosize scale.

The persistence of a dispersive spin-wave curve in the small- q range, which exists in the whole doping range up to $x_{Ca} = 0.22$, whatever the CAF or the F state, indicates that this charge segregation does not correspond to a phase separation into two distinct F states, but rather to a F state with two coupled components. The magnetic coupling involved in the dispersive branch, is responsible for the onset of 3D long-range F correlations (Bragg peaks) at T_C .

Finally, a magnon–phonon coupling is suggested, especially in the case of $\text{La}_{0.875}\text{Sr}_{0.125}\text{MnO}_3$, although not evidenced by polarized neutrons. Further experiments in applied field are planned to confirm its existence.

In conclusion, the most prominent feature deduced from the observation of the spin-wave excitations at the approach of the metallic state, is a charge segregation. This charge segregation occurs actually in the whole concentration range preceding the genuine ‘metallic’ state, although its nature may differ within this range. The size of the orbital-ordered domains in $\text{La}_{0.8}\text{Ca}_{0.2}\text{MnO}_3$, at a concentration very close to the metallic state ($x_{Ca} = 0.225$), recalls observations reported in the concentration range where CMR properties are observed. There, at the approach of T_C , several experiments have indicated the existence of an inhomogeneous state with clusters of similar size [54, 55]. If this relation is right, the present observations could be crucial for the understanding of these CMR properties.

Acknowledgments

The authors are very indebted to P Lehouelleur, A Ivanov, L P Regnault, J Kulda for their contribution and for fruitful discussions. They acknowledge J M Mignot and B Hennion for their critical reading of the manuscript. They are also very indebted to D Khomskii, K Kugel, and A M Oleś for enlightening discussions.

References

- [1] Zener C 1951 *Phys. Rev.* **81** 440
Zener C 1951 *Phys. Rev.* **82** 403
- [2] Millis A J, Littlewood P B and Shraiman B I 1995 *Phys. Rev. Lett.* **74** 5144
Millis A J, Littlewood P B and Shraiman B I 1998 *Nature* **392** 147
- [3] Nagaev E L 1970 *Sov. Phys.—JETP* **30** 693
- [4] Kasuya T, Yanase A and Takeda T 1970 *Solid State Commun.* **8** 1543
- [5] Kagan M Yu, Khomskii D I and Mostovoy M V 1999 *Eur. Phys. J. B* **12** 217
- [6] Arovas D and Guinea F 1998 *Phys. Rev. B* **58** 9150
- [7] Moreo A, Yunoki S and Dagotto E 1999 *Science* **283** 2034
- [8] de Gennes P G 1960 *Phys. Rev. B* **118** 141
- [9] Vasiliu-Doloc L, Lynn J, Moudden A H, de Leon-Guevara A M and Revcolevschi A 1998 *Phys. Rev. B* **58** 14913
- [10] Rodriguez-Carvajal J, Hennion M, Moussa F, Moudden A H, Pinsard L and Revcolevschi A 1998 *Phys. Rev. B* **57** 3189
- [11] Horsh P, Jaklic J and Mack F 1999 *Phys. Rev. B* **59** 6217
- [12] Khaliullin G and Kilian R 2000 *Phys. Rev. B* **61** 3494
- [13] Oleś A M and Feiner L F 2002 *Phys. Rev. B* **65** 52414
- [14] Moussa F, Hennion M, Biotteau G, Rodríguez-Carvajal J, Pinsard L and Revcolevschi A 1996 *Phys. Rev. B* **54** 15149
- [15] Hirota K, Kaneko N, Nishizawa A and Endoh Y 1996 *J. Phys. Soc. Japan* **65** 3736
- [16] Hennion M, Moussa F, Rodríguez-Carvajal J, Pinsard L and Revcolevschi A 1998 *Phys. Rev. Lett.* **81** 1957
- [17] Hennion M, Moussa F, Biotteau G, Rodríguez-Carvajal J, Pinsard L and Revcolevschi A 2000 *Phys. Rev. B* **61** 9513
- [18] Moussa F, Hennion M, Biotteau G, Rodríguez-Carvajal J, Pinsard L and Revcolevschi A 1999 *Phys. Rev. B* **60** 12299
- [19] Kober-Lehouelleur P, Moussa F, Hennion M, Ivanov A, Pinsard L and Revcolevschi A 2004 *Phys. Rev. B* **70** 144409
- [20] Biotteau G, Hennion M, Moussa F, Rodriguez-Carvajal J, Pinsard L, Revcolevschi A, Mukovschii Y M and Shulyatev D 2001 *Phys. Rev. B* **64** 104421
- [21] Feiner L F and Olés A 1999 *Physica B* **259–261** 796
- [22] Gork'ov L P and Kresin V Z 1998 *Pis. Zh. Eksp. Teor. Fiz.* **67** 934
Gork'ov L P and Kresin V Z 1998 *Pis. JETP Lett.* **67** 985
- [23] Pinsard L, Rodríguez-Carvajal J, Moudden A H, Anane A, Revcolevschi A and Dupas C 1997 *Physica B* **234–236** 856
- [24] Okuda T, Tomioka Y, Asamitsu A and Tokura Y 2000 *Phys. Rev. B* **61** 8009
- [25] Markovitch V, Rozenberg E, Shames A I, Gorodetsky G, Fita I, Suzuki K, Puzniak R, Shulyatev A A and Mukovskii Ya M 2002 *Phys. Rev. B* **65** 144402
- [26] Palstra T T M, private communication
- [27] Yamada Y, Hino O, Nohdo S, Kanao R, Inami T and Katano S 1996 *Phys. Rev. Lett.* **77** 904
- [28] Yamada Y, Susuki J, Oikawa K, Katano S and Fernandez-Baca J A 2000 *Phys. Rev. B* **62** 11600

- [29] Urushibara A, Moritomo Y, Arima T, Asamitsu A, Kido G, Tokura Y 1995 *Phys. Rev. B* **51** 14103
- [30] Kawano H, Kajimoto R, Kubota M and Yoshizawa H 1996 *Phys. Rev. B* **53** R14709
- [31] Moritomo Y, Kuwahara H, Tomioka Y and Tokura Y 1997 *Phys. Rev. B* **55** 7549
- [32] Zhou J S, Goodenough J B, Asamitsu A and Tokura Y 1997 *Phys. Rev. Lett.* **79** 3234
- [33] Senis R, Laukhin V, Martinez B, Fontcuberta J, Obrador X, Arsenov A A and Mukovskii Y M 1998 *Phys. Rev. B* **57** 14680
- [34] Endoh Y, Hirota K, Ishihara S, Okamoto S, Murakami Y, Nishizawa A, Fukuda T, Nojiri H, Kaneko K and Maekawa S 1999 *Phys. Rev. Lett.* **82** 4328
- [35] Cox D E, Iglesias T, Moshopoulou E, Hirota K, Takahashi K and Endoh Y 2001 *Phys. Rev. B* **64** 0244311
- [36] Ahn K H and Millis A J 1998 *Phys. Rev. B* **58** 3697
- [37] Mizokawa T, Khomskii D I and Sawatsky G A 2000 *Phys. Rev. B* **61** R3776
- [38] Klingeler R, Geck J, Gross R, Pinsard-Gaudart L, Revcolevschi A, Ulhenbruck S and Buchner B 2002 *Phys. Rev. B* **65** 174404
- [39] Geck J, Wochner P, Kiele S, Klingeler R, Revcolevschi A, Zimmermann M v, Buchner B and Reutler P 2004 *New J. Phys.* **6** 152
- [40] Dai P, Fernandez-Baca J A, Wakabayashi N, Plummer E W, Tomioka Y and Tokura Y 2000 *Phys. Rev. Lett.* **85** 2553
- [41] Adams C P, Lynn J W, Mukovskii Y M, Arsenov A A and Shulyatev D A 2000 *Phys. Rev. Lett.* **85** 3954
- [42] Papavassiliou G, Belesi M, Fardis M, Pissas M, Dolinsek J, Dimitropoulos C and Ansermet J P 2000 *Phys. Rev. Lett.* **84** 761
- [43] Chechersky V, Nath A, Isaac I, Franck J P, Ghosh K and Greene R L 2000 *Phys. Rev. B* **63** 052411
- [44] Laiho R, Landeranta E, Salminen J, Lisunov K G and Zakhvalinskii V S 2001 *Phys. Rev. B* **63** 094405
- [45] Moussa F, Hennion M, Wang F, Kober P, Rodríguez-Carvajal J, Reutler P, Pinsard L and Revcolevschi A 2003 *Phys. Rev. B* **67** 214430
- [46] Hennion M, Moussa F, Lehouelleur P, Wang F, Ivanov A, Mukovskii Y M and Shulyatev D 2005 *Phys. Rev. Lett.* **94** 057006
- [47] Mirebeau I, Hennion M, Casalta H, Andres H, Gudel H U, Irodova A V and Caneschi A 1999 *Phys. Rev. Lett.* **83** 628
- [48] Dai Pengcheng, Hwang H Y, Zhang J, Fernandez-Baca J A, Cheong S-W, Kloc C, Tomioka Y and Tokura Y 2000 *Phys. Rev. B* **61** 9553
- [49] Reichardt W and Braden M 1999 *Physica B* **263–264** 416
- [50] Kober-Lehouelleur P 2004 *Thesis* Université Paris-Sud
- [51] Hendriksen P V, Linderorth S and Lindgård P A 1993 *Phys. Rev. B* **48** 7259
- [52] Khomskii D I and Kugel K I 2003 *Europhys. Lett.* **55** 208
- [53] Biotteau G 2000 *Thesis* Université Paris VII
- [54] Lynn J W, Erwin R W, Borchers J A, Huang Q, Santoro A, Peng J L and Li Z Y 1996 *Phys. Rev. Lett.* **76** 4046
- [55] de Teresa J M, Ibarra M R, Algarabel P A, Ritter C, Marquina C, Blasco J, Garcia J, del Moral A and Arnold Z 1997 *Nature* **386** 256